Analytical Thermal Cable Models for Ampacity Derating Calculation in Smart Fuses

Analytische thermische Kabelmodelle für die Berechnung der Strombelastbarkeit in intelligenten Sicherungen

Anika Henke, Stephan Frei, TU Dortmund

Abstract

In modern vehicles, the cable harness complexity still increases due to the rising amount of functions. In addition, higher reliability demands occur. As the insulation temperature highly influences the cable aging, thermal considerations play an important role with respect to the reliability of the system. The cable aging process can be monitored by applying intelligent fusing strategies based on the known cable temperature. The calculation of the axial transient temperature distribution in cable structures is a complex task that is often solved numerically. In this paper, an analytical approach to model the temperature of a single cable in air is presented based on a calculation in the Laplace domain. Switching on and off of the load current is considered, which enables the calculation of the temperature distribution during the cable heating and cool down. The approach is validated using a numerical reference solution and measurement results. As further application the monitoring of the cable aging is discussed.

Kurzfassung

Aufgrund der zunehmenden Anzahl an Funktionen nimmt die Komplexität des Kabelbaumes in modernen Kraftfahrzeugen noch immer zu. Zusätzlich steigen die Anforderungen an die Zuverlässigkeit. Da die Temperatur der Kabelisolierung stark das Alterungsverhalten der Leitungen beeinflusst, sind thermische Betrachtungen für die Beurteilung der Zuverlässigkeit des Systems von großer Bedeutung. Die Alterung im Kabel kann durch die Anwendung von intelligenten Sicherungskonzepten basierend auf der bekannten Kabeltemperatur überwacht werden. Die Berechnung der axialen transienten Temperaturverteilung in Leitungsstrukturen ist eine herausfordernde Aufgabe, die häufig numerisch gelöst wird. In diesem Beitrag wird ein analytischer Ansatz für die Temperaturberechnung für eine ungeschirmte Einzelleitung in Luft unter Verwendung der Laplace-Transformation präsentiert. Der Temperaturverlauf im Aufheiz- und Abkühlungsprozess nach Ein- und Ausschalten des Laststromes wird modelliert. Die Validierung erfolgt mit Hilfe einer numerischen Referenzlösung und mit Messergebnissen. Als weitere Anwendung wird die Überwachung der Alterung einer Leitung diskutiert.

1 Introduction

In the cable harness development process maximum currents must be estimated and the cable has to be dimensioned accordingly. The design must avoid overload under normal conditions. Once under operation, the cable has to be protected from damage caused by high temperatures. Classically, melting fuses are used to fulfill this task. An exemplary application in a vehicle is shown in Figure 1. Those melting fuses cannot meet the growing requirements concerning diagnosis and reset functions [1]. That is why electronic fuses [2] (see Figure 1) were developed, that use smart fusing strategies. The tripping strategies of such fuses are based on insulation temperature estimations. In case of a too high temperature, the circuit is interrupted. For various reasons, often, it is not possible to measure the cable temperature directly. Indirect model-based approaches for a current based ampacity calculation are more feasible.

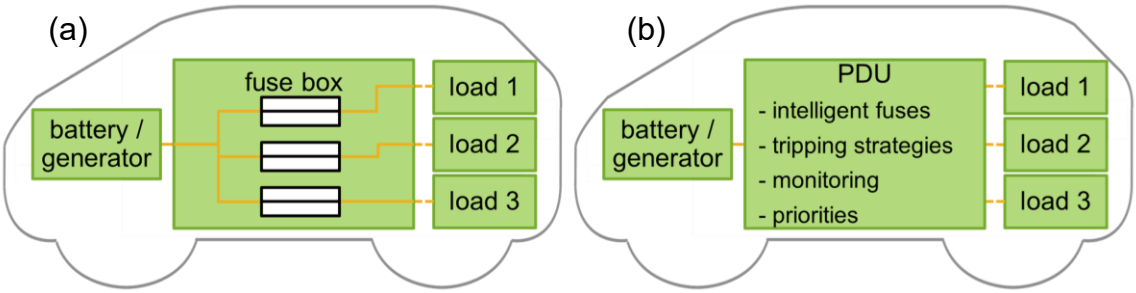

Figure 1: (a) Melting fuses and (b) smart fuses in vehicular application.

Since fuses are very cost sensitive components, the needed computing power has to be low. Computationally efficient models are required. That is why numerical methods can be critical.

Several electrothermal cable models were developed in the past, for example in [3, 4, 5], with strongly varying properties. Previous works frequently used radial thermal cable models [6, 7]. Modelling only the radial heat flow through the cable means neglecting the axial heat flow. Those models lead to a good approximation of the temperature for long cables with negligible influence of the beginning and the end of the cable. In real applications, the cable terminations affect the cable temperature and provide important boundary conditions. Neglecting those may lead to high calculation errors. That is why the axial heat flow needs to be considered to get results that are more precise. Furthermore, especially for short cables, the ampacity might be significantly higher than a calculation with a radial model would estimate if the contacts cool the cable. To consider this and exploit more of the cable's current carrying capacity, axial cable models can be advantageous, which leads to more complex models, see for example [8]. Another property that influences the complexity of the model is whether or not the time dependency is considered. Since high currents can be tolerated through the cable for a short period of time, transient models as for example in [4] and [9] are necessary. Classically, models that consider the axial as well as transient temperature development are based on numerical approaches. In this paper, an analytical approximation for the axial transient temperature distribution in an insulated cable is presented.

As shown for example in [10], the electrical transmission line theory can be adapted for thermal investigations. There, an equivalent circuit for an infinitesimally short cable segment is used to derive a differential equation. The axial voltage respectively current distributions are calculated as a solution of this differential equation [11]. This precede

is adapted for thermal investigations in [12] and extended in this contribution. As a result, the temperature at each position along the cable and each point in time can be calculated independently. An iterative approach is presented to consider nonlinear cable parameters.
In chapter 2, the fundamental model is presented. Earlier research is shortly summarized. The solution is expanded to enable the consideration of switching off the current in chapter 3. In chapter 4, the measurement procedure is presented and in chapter 5, the solution is validated using numerical reference solutions and measurement results. The applicability of the solution is discussed in chapter 6 using an application example. The results are summed up in chapter 7.

2 Analytical Calculation of Cable Heating

2.1 Fundamental Model

This chapter is based on [12]. There, a single cable of length L oriented in z-direction consisting of a conductor with the radius r_c and an insulation with the outer radius r_i as shown in Figure 2 is examined.

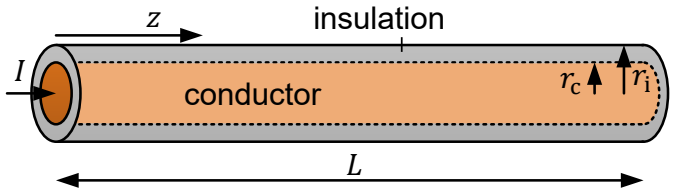

Figure 2: Analyzed single cable.

Analogously to the electrical transmission line theory, the equivalent circuit for an infinitesimally short cable segment shown in Figure 3 is used. The per unit length heat source P_e' represents the cable heating induced by the current I that flows through the conductor and depends on the conductor temperature T. The per unit length capacitance C' is used to model the heat storing capacity of the complete cable (conductor and insulation). The per unit length admittance G' describes the heat conduction through the insulation layer and the heat transfer from the cable to the ambient air via convection and radiation and therefore depends on the cable surface temperature T_s and the ambient air temperature T_e. The axial heat flow in the conductor is modelled using the per unit length resistance R'. The axial heat flow in the insulation is neglected due to the low thermal conductivity of the insulation compared to the conductor.

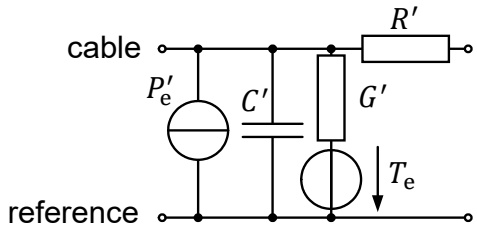

Figure 3: Thermoelectric equivalent circuit for an infinitesimally short cable segment.

From this equivalent circuit, the partial differential equation is derived for the conductor temperature T:

$$\frac{\partial^2 T(z,t)}{\partial z^2} - A\frac{\partial T(z,t)}{\partial t} - BT(z,t) = C \tag{1}$$

with

$$A = R'C', \quad B = R'G', \quad C = R'(P_\mathrm{e}' - G'T_\mathrm{e}). \tag{2}$$

As initial and boundary conditions, constant temperatures are assumed:

$$T(z,0) = T_0, \quad T(0,t) = T_1, \quad T(L,t) = T_2. \tag{3}$$

2.2 Solution of the Differential Equation via Laplace Transform

This differential equation is solved in [12] using the Laplace transform. In the Laplace domain, the corresponding ordinary differential equation is solved analytically. Using the approximation

$$e^{-L\sqrt{sA+B}} \pm 1 \approx \pm 1, \tag{4}$$

which is valid for large L, an analytical expression in the time domain is calculated:

$$\begin{aligned} T(z,t) = &-\frac{C}{B} - \left(\frac{C}{B} + T_0\right)\Xi(t)[1 - \Lambda(z_\mathrm{L},t) - \Lambda(z,t)] \\ &- \frac{1}{2}\left[\left(\frac{C}{B} + T_1\right)\Gamma(z,t) + \left(\frac{C}{B} + T_2\right)\Gamma(z_\mathrm{L},t)\right] \end{aligned} \tag{5}$$

with

$$\begin{aligned} \Lambda(z,t) &= \mathrm{erf}\left(\frac{z}{2}\sqrt{\frac{A}{t}}\right), \quad \Xi(t) = e^{-\frac{B}{A}t}, \quad z_\mathrm{L} = L - z, \\ \Gamma(z,t) &= \left[\mathrm{erf}\left(\frac{Az - 2t\sqrt{B}}{2\sqrt{At}}\right) - 1\right]e^{-z\sqrt{B}} + \left[\mathrm{erf}\left(\frac{Az + 2t\sqrt{B}}{2\sqrt{At}}\right) - 1\right]e^{z\sqrt{B}}. \end{aligned} \tag{6}$$

This solution is validated using a numerical reference solution in [12].

2.3 Iterative Approach to Include Nonlinear Parameters

As already mentioned above, the parameters P_e' and G' in the equivalent circuit are not constant but depend on the cable and surface temperatures. This nonlinear component was neglected in the above presented solution. To take it into account, an iterative solution approach is developed in [12] and is shortly resumed here: After an initialization, the surface temperature and the parameters are calculated. Those are used to find the conductor temperature. As termination condition, the absolute difference $\sigma_\mathrm{T} =$

$|T^k - T^{k+1}|$ between two iterations is calculated. The process is continued until this difference falls below $\Delta_{\mathrm{T,Limit}} = 0.001\ \mathrm{K}$. In Figure 4, this approach is summed up.

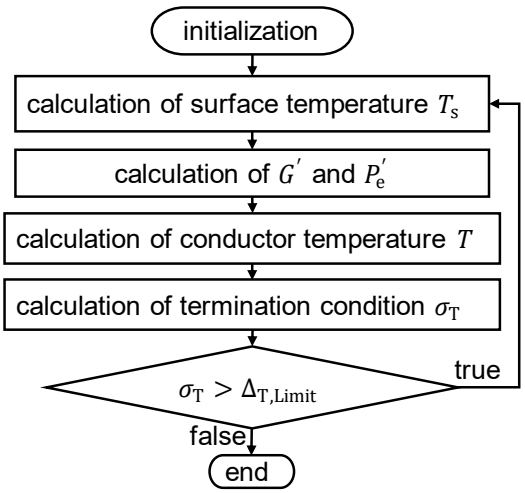

Figure 4: Iterative approach to consider nonlinear parameter dependencies.

2.4 Expansion for Current Switch-Off

Till now, solutions were only available for a constant current excitation that is switched on at $t = 0$ [12]. Here, an expansion is developed that allows switching off the current I_0 at the time $\hat{t}$. So, the time-dependent current follows a rectangular shape:

$$I(t) = I_0 \hat{t} \mathrm{rect}_{\hat{t}}\left(t - \frac{\hat{t}}{2}\right). \tag{7}$$

Therefore, the heat source P_e' also follows a rectangular shape:

$$P_e'(t) = I^2(t) R_{\mathrm{ref}}'\left(1 + \alpha_T (T - T_{\mathrm{ref}})\right) = P_0' \hat{t} \mathrm{rect}_{\hat{t}}\left(t - \frac{\hat{t}}{2}\right). \tag{8}$$

α_T is the linear temperature coefficient for the conductor's conductivity, and R_{ref}' represents the electric per unit length resistance at the temperature T_{ref}. The new partial differential equation is

$$\frac{\partial^2 T(z,t)}{\partial z^2} - A \frac{\partial T(z,t)}{\partial t} - B T(z,t) = C_1 + C_2 \cdot \hat{t} \mathrm{rect}_{\hat{t}}\left(t - \frac{\hat{t}}{2}\right) \tag{9}$$

with

$$C_1 = -R' G' T_e, \quad C_2 = R' P_0'. \tag{10}$$

Again, the solution is calculated using the Laplace domain. For the analytical transformation back into the time domain, the approximation (4) is used. The complete expression in the time domain is

$$T_{\mathrm{on}}(z,t) = -\frac{C_1+C_2}{B} - \left(\frac{C_1+C_2}{B} + T_0\right)\Xi(t)[1-\Lambda(z_{\mathrm{L}},t)-\Lambda(z,t)] - \frac{1}{2}\left[\left(\frac{C_1+C_2}{B}+T_1\right)\Gamma(z,t) + \left(\frac{C_1+C_2}{B}+T_2\right)\Gamma(z_{\mathrm{L}},t)\right] \tag{11}$$

for $0 \leq t < \hat{t}$ and

$$T_{\mathrm{off}}(z,t) = T_{\mathrm{on}}(z,t) - \frac{C_2}{B}\left\{1 + \Xi(t-\hat{t})[1-\Lambda(z_{\mathrm{L}},t-\hat{t})-\Lambda(z,t-\hat{t})] + \frac{1}{2}[\Gamma(z_{\mathrm{L}},t-\hat{t})+\Gamma(z,t-\hat{t})]\right\} \tag{12}$$

for $t \geq \hat{t}$.

3 Measurement Methods for Thin Cables

The calculated temperature distributions are compared to real measurement results. In this chapter, two measurement techniques for thin cables are presented.
In many applications, the temperature resilience of the insulation is critical. That is why the warmest position along the insulation has to be found. In typical environments, the surrounding air cools the cable, which means that the hottest spot of the insulation is at the transition to the inner conductor. So, the conductor temperature is relevant.
The cable heats up the environmental air, so the ambient temperature varies during the measurement. Therefore, this temperature is measured additionally to the cable temperature.

3.1 Indirect Temperature Measurement

The indirect temperature measurement (see also [13]) is based on the measurement of the cable resistance: As the resistance of the cable depends on its temperature, the measurement of the cable resistance allows conclusions about the cable temperature. Because of the assumed low temperature rises, it is often sufficient to consider the linear temperature coefficient:

$$R_{\mathrm{cable}} = R_{\mathrm{ref}}\left(1+\alpha_{\mathrm{T}}(T-T_{\mathrm{ref}})\right) \Leftrightarrow T - T_{\mathrm{ref}} = \frac{1}{\alpha_{\mathrm{T}}}\left(\frac{R_{\mathrm{cable}}}{R_{\mathrm{ref}}} - 1\right). \tag{13}$$

The cable resistance is calculated from the current, that is injected by a current source into the cable, and the voltage drop across the measured cable section. Using this approach, the mean cable temperature across the section for the voltage measurement is calculated. That is why this measurement method is used to measure the temperature over time in the middle of a sufficiently long cable: Across the middle section of the length L_{meas}, where the temperature and therefore the resistance is approximately constant, the measurement is done. The measurement current I_{meas} is injected into the cable directly at the current source. That is to avoid an additional voltage drop across the contacts for the voltage measurement, which would be measured as well and therefore distort the measurement. The measurement method is shown in Figure

5. In total, the complete current flowing through the cable becomes $I + I_{\mathrm{meas}}$, and, obviously, the load current I also (highly) influences the measured voltage drop.

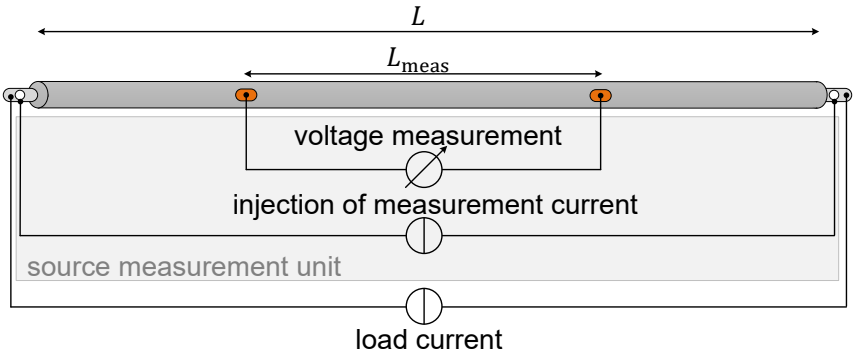

Figure 5: Scheme for the measurement setup.

To eliminate this influence, a differential measurement is used: The voltage is measured three times. In the first and the third measurement, the negative measurement current $-I_{\mathrm{meas}}$ is used, in the second measurement, the positive current $+I_{\mathrm{meas}}$ is used. Using the first and third measurement and a linear interpolation as depicted in Figure 6, the corresponding voltage for negative measurement current at the time of the measurement with positive current is approximated. Then, the difference between the voltage measured with positive measurement current and this approximated corresponding voltage for negative measurement current only depends on the measurement current and no longer on the load current. In addition, a possible zero-point error of the measurement device is eliminated by only evaluation voltage differences. The measured resistance therefore is

$$R_{\mathrm{cable}} = \frac{2U_2 - U_1 - U_3}{2I_2 - I_1 - I_3} = \frac{2U_2 - U_1 - U_3}{4I_{\mathrm{meas}}}. \tag{14}$$

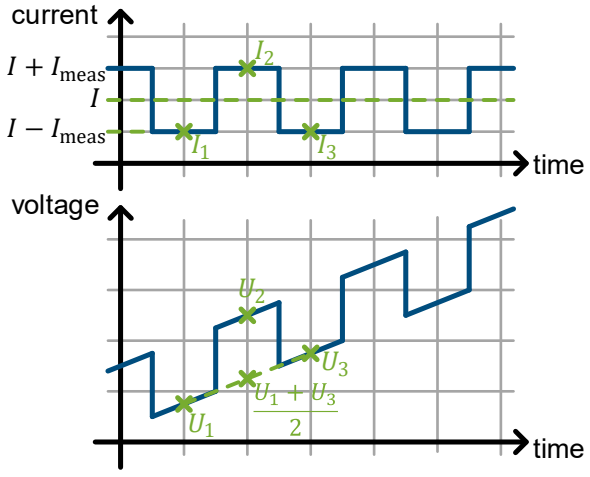

Figure 6: Measurement procedure for the resistance calculation.

At first, the reference resistance is measured without load current. The reference temperature is the environmental temperature during this measurement. In the next step, the load current is switched on and the actual measurement of the cable resistance for the calculation of the cable temperature is performed. If the section for the voltage

measurement is too short the measured voltage drop is small and the measurement errors can be high. That is why in general, this method is only applicable to longer cable sections with constant temperature.

3.2 Thermocouples

The axial cable temperature distribution is measured using thermocouples (type K). Those have to be connected to the conductor. The measured temperature is highly dependent on the quality of the connection between the cable and the thermocouple. If galvanically coupled thermocouples are used, the thermocouples themselves have to be installed electrically insulated from the conductor potential. Nevertheless, a good thermal coupling between thermocouple and conductor is essential for a precise temperature measurement. In this case, for example Kapton tape (electrically insulating, thermally conductive) can be placed in between the conductor and the thermocouple. Heat-conducting paste is used to further improve the thermal coupling. The thermocouple leads away heat from the conductor itself and therefore influences the measurement. As its diameter is small in comparison with the diameter of the conductor, this effect can be neglected here.

4 Validation

In this section, the previously derived calculation formulas are validated using a numerical reference solution and measurement results. The numerical solution is found by using the partial differential equation that describes the problem and solve it by using the function “pdepe” of MATLAB [14].
A $1.5\ \mathrm{mm}^2$ copper cable (specific heat capacity $c_\mathrm{c} = 3.4 \cdot 10^6\ \mathrm{J/m^3K}$, thermal conductivity $\lambda_\mathrm{c} = 386\ \mathrm{W/Km}$, resistivity at $20\ °\mathrm{C}$ $\rho = 1.86 \cdot 10^{-8}\ \Omega\mathrm{m}$, linear temperature coefficient $\alpha_\mathrm{T} = 3.93 \cdot 10^{-3}\ 1/\mathrm{K}$) with PVC insulation (total radius with insulation $r_\mathrm{i} = 1.7\ \mathrm{mm}$, specific heat capacity $c_\mathrm{i} = 2.245 \cdot 10^6\ \mathrm{J/m^3K}$, thermal conductivity $\lambda_\mathrm{i} = 0.21\ \mathrm{W/Km}$, emissivity $\varepsilon = 0.95$) and the length $L = 1.5\ \mathrm{m}$ is examined. This cable is connected to massive copper plates at the cable ends to hold the cable end temperatures at constant values during the short measurements. Between the positions $z = 0.35\ \mathrm{m}$ and $z = 1.15\ \mathrm{m}$, the indirect temperature measurement is performed. Thermocouples are connected to the conductor at $z = 5\ \mathrm{cm}$, $z = 10\ \mathrm{cm}$ and $z = 75\ \mathrm{cm}$. At the time $t = 0\ \mathrm{s}$, the current $I = 30\ \mathrm{A}$ is switched on and at the time $t = 490\ \mathrm{s}$ it is switched off again. In Figure 7, the complete experimental setup is shown.
In the cable modelling, a massive conductor is assumed. In real applications, often flexible cables are used. Then, the conductor consists of several braids with small air gaps in between. That is why in the modelling the differentiation between an effective copper cross section with a corresponding radius and the geometrical cross section that is filled with copper and air needs to be used. The examined flexible $1.5\ \mathrm{mm}^2$-cable consists of 30 braids with a diameter of $d_\mathrm{braid} = 0.25\ \mathrm{mm}$. The complete area, that is filled with copper, therefore is

$$A_\mathrm{Cu} = 30 \cdot \pi \cdot \left(\frac{d_\mathrm{braid}}{2}\right)^2 \approx 1.47\ \mathrm{mm}^2, \tag{15}$$

which leads to an effective copper radius of

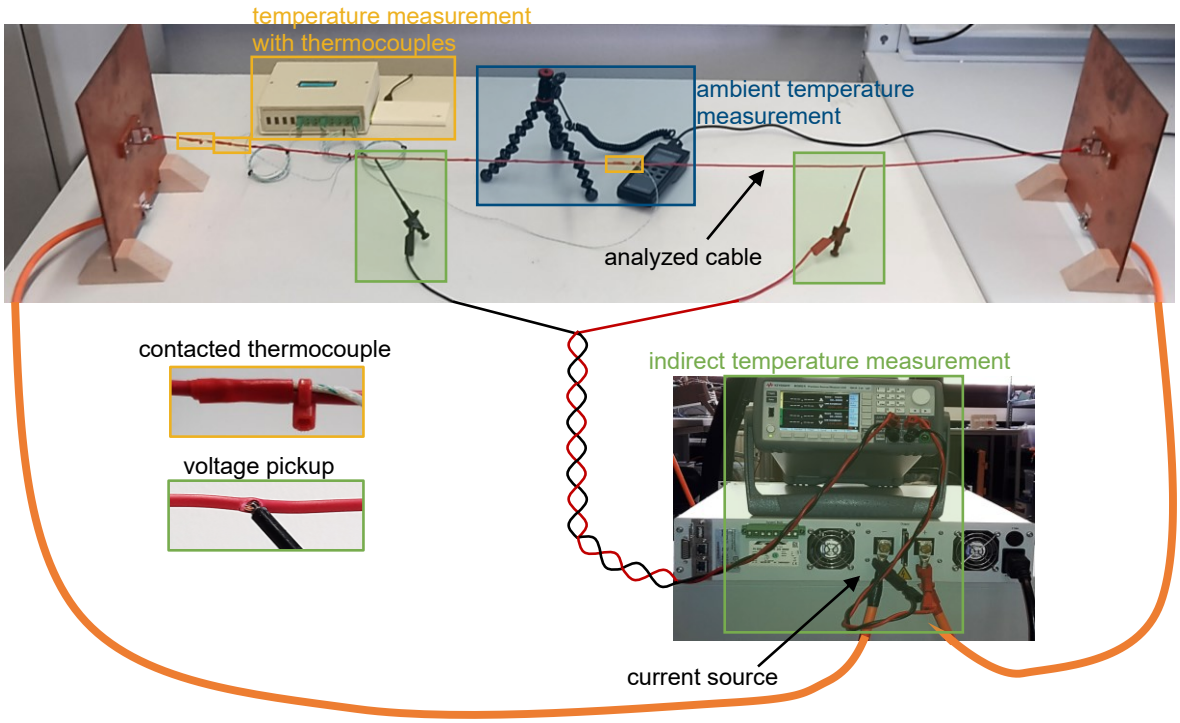

Figure 7: Experimental setup that combines the indirect temperature measurement and the temperature measurement with thermocouples.

$$r_{\mathrm{c,eff}} = \sqrt{\frac{A_{\mathrm{Cu}}}{\pi}} = \sqrt{7.5} \cdot d_{\mathrm{braid}} \approx 0.68\ \mathrm{mm}. \tag{16}$$

This effective radius is used for the calculation of the parameters that characterize the conductor:

$$C_{\mathrm{c}}' = c_{\mathrm{c}} \pi r_{\mathrm{c,eff}}^2, \quad R' = \frac{1}{\lambda_{\mathrm{c}} \cdot \pi \cdot r_{\mathrm{c,eff}}^2}. \tag{17}$$

λ_{c} is the thermal conductivity of the conductor. c_{c} is the specific heat capacity per volume that is used to calculate the thermal per unit length capacitance for the conductor C_{c}'. Together with the corresponding capacitance for the insulation C_{i}', the complete cable capacitance results as

$$C' = C_{\mathrm{c}}' + C_{\mathrm{i}}'. \tag{18}$$

For the parameters describing the insulation, the inner radius of the insulation is relevant. The outer radius of the complete cable with insulation $r_{\mathrm{i}} = 1.7\ \mathrm{mm}$. The thickness of the insulation layer is $d_{\mathrm{i}} = 0.7\ \mathrm{mm}$. This leads to the inner radius of the insulation $r_{\mathrm{c,geom}}$:

$$r_{\mathrm{c,geom}} = r_{\mathrm{i}} - d_{\mathrm{i}} = 1\ \mathrm{mm}. \tag{19}$$

This value is used in the calculation of the parameters for the insulation:

$$R'_\lambda = \frac{\ln\left(\frac{r_\mathrm{i}}{r_\mathrm{c,geom}}\right)}{2\pi\lambda_\mathrm{i}}, \quad C'_\mathrm{i} = c_\mathrm{i}\pi\left(r_\mathrm{i}^2 - r_\mathrm{c,geom}^2\right). \tag{20}$$

λ_i is the thermal conductivity of the insulation and c_i is the thermal conductivity of the insulation. The thermal per unit length resistance R'_λ describes the heat transfer through the insulation. Together with the thermal per unit length resistance R'_α, that is used to model the heat transfer between the surface of the cable and the surrounding air, the parameter G' of the partial differential equation results:

$$G' = \frac{1}{R'_\lambda + R'_\alpha}. \tag{21}$$

In the above-mentioned calculation of the per unit length resistance R'_λ, that describes the heat flow through the insulation, the insulation is assumed to be a perfect hollow cylinder. In the real cable, the insulation follows the structure defined by the braids and therefore differs significantly from this assumption. In Figure 8, a picture of the cross section of the insulation is shown.

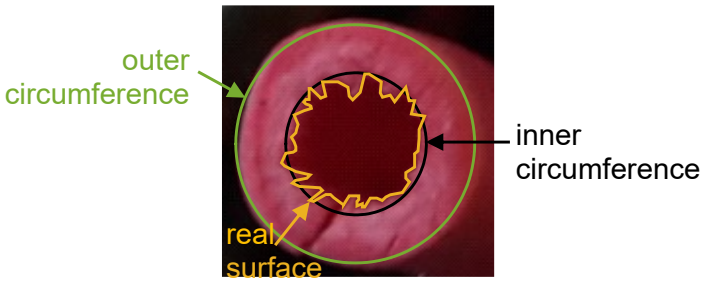

Figure 8: Cross section of the insulation with the assumed outer circumference (green), inner circumference (black) and the real inner surface (yellow).

The green circle represents the outer circumference of the insulation and the black circle shows the assumed inner circumference of the insulation. Graphically, the real inner surface of the insulation is emulated (yellow curve in Figure 8). As the yellow curve is much longer than the black one, the coupling area between the conductor and the insulation is much higher than assumed before. Here, it is assumed that the heat flow is depending on the coupling area. Thus, the correction factor F for the per unit length resistance R'_λ is introduced and estimated as the relation between the lengths of the black and the yellow curve in Figure 8:

$$F \approx 0.69 \Rightarrow R'_\mathrm{\lambda,corr} = F \cdot R'_\lambda \tag{22}$$

As the voltage measurement data is noisy due to the low voltage drop the measured data has to be filtered by a floating average filter.
The ambient temperature varies during the measurement as the cable heats up the environmental air as shown in Figure 9. As the environmental temperature does not vary much during the measurement, in the simulation, a constant temperature of $25\ °\mathrm{C}$ is assumed.

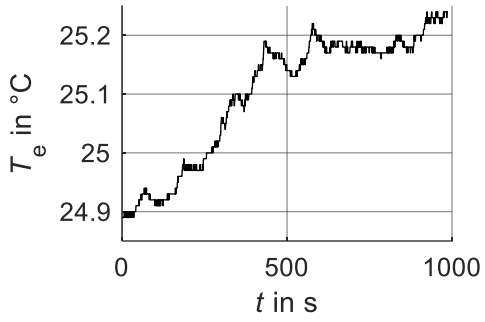

Figure 9: Environmental temperature development during the measurement.

The temperatures at the beginning and the end of the cable and the initial cable temperature are set to the value of the ambient temperature. In Figure 10, the results are shown and the agreement between the measured and the calculated temperature development is good.

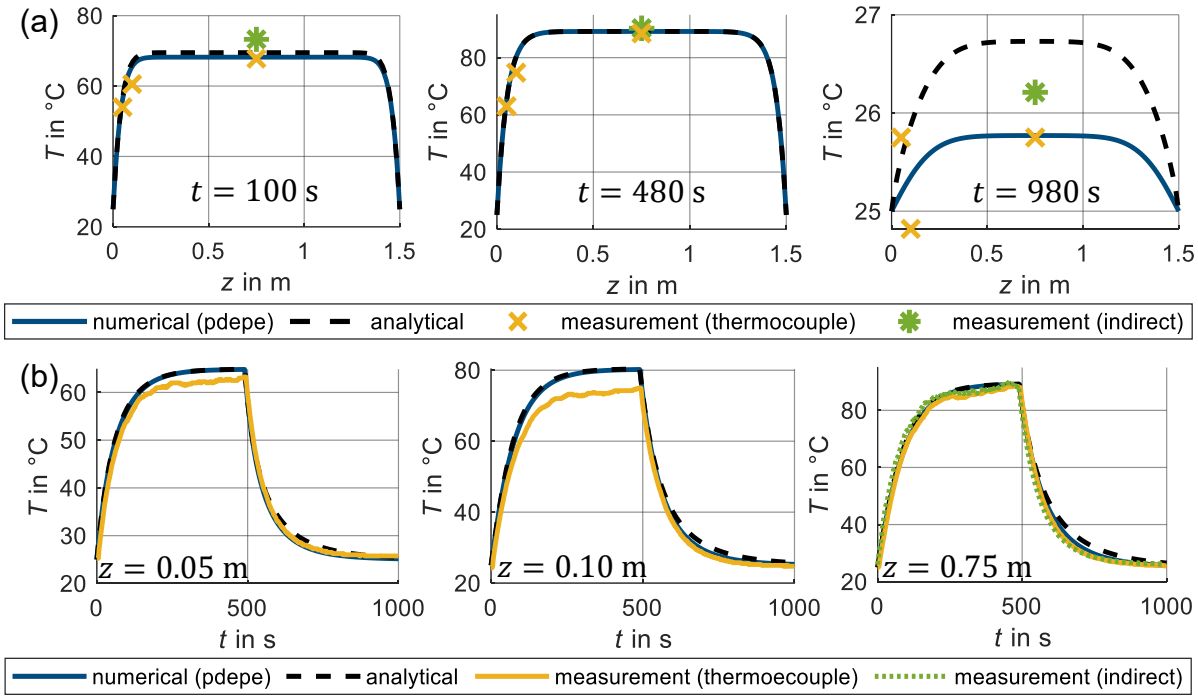

Figure 10: Numerically and analytically calculated and measured temperature developments for fixed (a) times and (b) spatial positions.

5 Application Example

Higher insulation temperatures lead to an accelerated cable aging. Intelligent fuses enable the sophisticated monitoring of this aging process and extend the application range of a cable. Short-term overload situations can be tolerated. This is practically relevant especially for safety-critical tasks. In this chapter, the previously presented and validated methods are applied for this task. In the standard ISO 6722, for PVC,

the continuous operation temperature $T_{3000\mathrm{h}} = 105\ °\mathrm{C}$, i.e. the cable can stand a temperature of $105\ °\mathrm{C}$ for 3000 hours, and the thermal overload temperature (6 hours) $T_{6\mathrm{h}} = 155\ °\mathrm{C}$ are defined. Generally, the cable insulation aging p_{aging} can be calculated from the cable temperature in Kelvin T_{K} using the Arrhenius equation in combination with Miner's rule [15] as also proposed in [13] and [16]:

$$p_{\mathrm{aging}} = \int_{t=0}^{t_{\mathrm{end}}} \frac{1}{A_{\mathrm{ar}}} e^{-\frac{b_{\mathrm{ar}}}{T_{\mathrm{K}}(t')}}\,\mathrm{d}t'. \tag{23}$$

The parameters A_{ar} and b_{ar} are calculated by inserting the two values $T_{3000\mathrm{h}}$ and $T_{6\mathrm{h}}$ into this equation:

$$\begin{aligned} b_{\mathrm{ar}} &= \frac{\ln\left(\frac{3000\ \mathrm{h}}{6\ \mathrm{h}}\right)}{\frac{1}{T_{3000\mathrm{h}}} - \frac{1}{T_{6\mathrm{h}}}} = 2.0124 \cdot 10^4\ \mathrm{K}, \\ A_{\mathrm{ar}} &= 3000\ \mathrm{h} \cdot e^{\frac{b_{\mathrm{ar}}}{T_{3000\mathrm{h}}}} = 1.393 \cdot 10^{-18}\ \mathrm{s}. \end{aligned} \tag{24}$$

Till now, cables are generally dimensioned to operate at temperatures below $T_{3000\mathrm{h}}$. With intelligent fuses unexpected overload situations with temporally limited higher temperatures can be considered and the remaining lifetime can be monitored. For temperatures lower than $T_{3000\mathrm{h}}$, the aging is estimated using the temperature $T_{3000\mathrm{h}}$.
Here, a single overload current pulse is assumed, that is switched on at the time $t = 0$ and lasts for the time t_{on}. Afterwards, the current is zero again. It is assumed that the cable cools down afterwards and is not loaded again during this cool-down process. At first, in the simulation, the end time is calculated, after which the cable temperature has cooled down to $T_{\mathrm{e}} + 1\ \mathrm{K}$ via the bisection method with a stop accuracy of $1\ \mathrm{s}$. Now, the aging for the complete process (heating up and cooling down again) is calculated. At first, it is calculated whether the critical insulation temperature (middle of the cable, as here, the highest temperatures appear) exceeds the value $T_{3000\mathrm{h}}$ at the end of the heating up process (time $t = t_{\mathrm{on}}$). If it does not, the aging is directly calculated via

$$p_{\mathrm{aging}} = \frac{1}{A_{\mathrm{ar}}} e^{-\frac{b_{\mathrm{ar}}}{T_{3000\mathrm{h}}}} \cdot t_{\mathrm{end}}. \tag{25}$$

If the temperature $T_{3000\mathrm{h}}$ is exceeded, in the next step, the times during the heating up and cooling down are calculated at which the cable temperature crosses the value $T_{3000\mathrm{h}}$ (bisection method). Outside these points, again, $T_{3000\mathrm{h}}$ is assumed for the aging calculation. In between these two points, the temperature development is approximated with rectangular shapes with the width Δt. In the middle of each interval (position t_i), the temperature T_i is calculated. Then, for the complete section with higher temperature than $T_{3000\mathrm{h}}$, the cable aging is calculated via

$$p_{\mathrm{aging},>T_{3000\mathrm{h}}} = \sum_i \frac{1}{A_{\mathrm{ar}}} e^{-\frac{b_{\mathrm{ar}}}{T_i}} \cdot \Delta t. \tag{26}$$

This method is applied for an exemplary setup in the following: A $4\ \mathrm{mm}^2$ copper cable with PVC insulation (total radius with insulation $r_{\mathrm{i}} = 1.7\ \mathrm{mm}$) and the length $L = 3\ \mathrm{m}$ is

loaded with the current $I = 36\,\mathrm{A}$ for $t_{\mathrm{on}} = 1200\,\mathrm{s}$. Worst case assumptions for the environmental temperature $T_{\mathrm{e}} = 85\,°\mathrm{C}$, the cable end temperatures $T_1 = T_2 = 85\,°\mathrm{C}$ and the cable start temperature $T_0 = 85\,°\mathrm{C}$ are taken into account. Along the cable, at the position $z = 1.5\,\mathrm{m} = L/2$ (cable middle), the highest temperatures appear. After $t_{\mathrm{end}} = 1717\,\mathrm{s}$, the cable has cooled down to $T_{\mathrm{e}} + 1\,\mathrm{K} = 86\,°\mathrm{C}$. That is why the calculation is stopped at this point. Between the times $91\,\mathrm{s}$ and $1262\,\mathrm{s}$, the cable temperature is higher than $T_{3000\mathrm{h}}$. Exemplarily, for presentation reasons the very rough discretization $\Delta t = 100\,\mathrm{s}$ is chosen for the aging calculation here. In Figure 11, the analytically calculated cable temperature, the approximated step function and the resulting calculated cable aging are shown. The complete process leads to about $4.2\,\%$ cable aging. For comparison, also, a lower current is evaluated: For $I = 18\,\mathrm{A}$, the temperature $T_{3000\mathrm{h}}$ is not exceeded. If this current lasts as before for $t_{\mathrm{on}} = 1200\,\mathrm{s}$, after $t_{\mathrm{end}} = 1525\,\mathrm{s}$ the cable has cooled down to $T_{\mathrm{e}} + 1\,\mathrm{K} = 86\,°\mathrm{C}$. This process only consumes about $0.85\,\%$ of the cable aging. So generally, many overload situations can be tolerated but lead to an accelerated cable aging. The cable aging has to be monitored to warn the user in case of depleted lifetime and ensure a safe operation at any time.

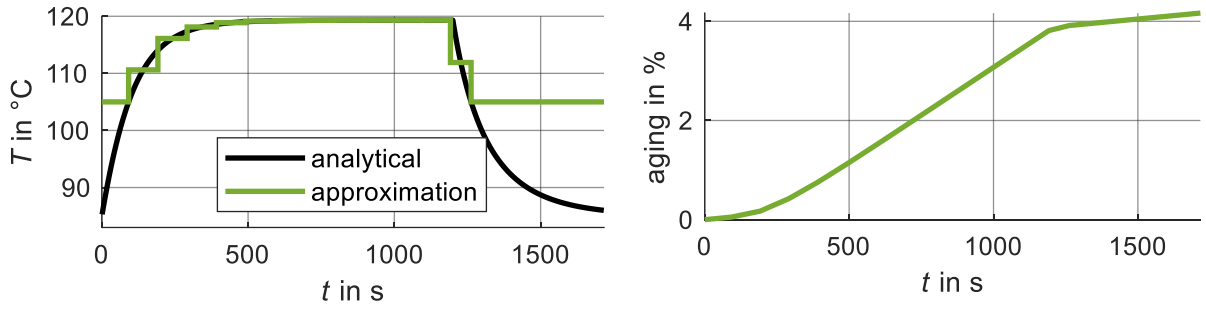

Figure 11: Analytical temperature development and approximation for cable aging calculation.

6 Conclusion

In this contribution, an analytical approach for the calculation of the axial and transient temperature development of a single unshielded cable was extended to also model the cooling down of the cable after the load current is switched off. The approach is validated using a numerical reference solution and measurement results. An example for the application for the cable aging monitoring is presented.

Acknowledgment

This work was supported in part by the European Fund for regional development (EFRE), Ministerium für Wirtschaft, Innovation, Digitalisierung und Energie of the State of North Rhine-Westphalia (MWIDE NRW) as part of the AFFiAncE project (EFRE-0801219).

References

[1] M. Horn, L. Brabetz and M. Ayeb, “Data-driven Modeling and Simulation of Thermal Fuses,” in *IEEE ESARS-ITEC*, Nottingham, U.K., 2018.

[2] S. Önal and S. Frei, “A model-based automotive smart fuse approach considering environmental conditions and insulation aging for higher current load limits and short-term overload operations,” in *IEEE ESARS-ITEC*, Nottingham, U.K., 2018.

[3] F. Loos, K. Dvorsky and H.-D. Liess, “Two approaches for heat transfer simulation of current carrying multicables,” *Math. Comput. Simul.,* vol. 101, pp. 13-30, 2014.

[4] Q. Zhan, J. Ruan, K. Tang, L. Tang, Y. Liu, H. Li and X. Ou, “Real-time calculation of three core cable conductor temperature based on thermal circuit model with thermal resistance correction,” *JoE,* vol. 2019, no. 16, p. 2036–2041, 2019.

[5] A. Ilgevicius, *Analytical and numerical analysis and simulation of heat transfer in electrical conductors and fuses,* Dissertation, Fakultät für Elektrotechnik und Informationstechnik, Universität der Bundeswehr, München, 2004.

[6] C. Holyk, H.-D. Liess, S. Grondel, H. Kanbach and F. Loos, “Simulation and measurement of the steady-state temperature in multi-core cables,” *Electr. Pow. Syst. Res.,* vol. 116, p. 54–66, 2014.

[7] S. L. Rickman und C. J. Iannello, „Heat transfer analysis in wire bundles for aerospace vehicles,“ in *Proc. 14th Int. Conf. HT*, Ancona, Italy, 2016.

[8] L. Brabetz, M. Ayeb und H. Neumeier, „A new approach to the thermal analysis of electrical distribution systems,“ in *SAE*, Detroit, MI, USA, 2011.

[9] R. Olsen, G. J. Anders, J. Holboell und U. S. Gudmundsdóttir, „Modelling of dynamic transmission cable temperature considering soil-specific heat, thermal resistivity, and precipitation,“ *IEEE Trans. Power Del.,* Bd. 28, Nr. 3, p. 1909–1917, 2013.

[10] P. Hui and H. S. Tan, “A transmission-line theory for heat conduction in multilayer thin films,” *IEEE Trans. Comp., Packag., Manufact. Technol. B,* vol. 17, no. 3, pp. 426-434, 1994.

[11] C. R. Paul, Analysis of multiconductor transmission lines, 2. ed., Piscataway, NJ, USA: IEEE Press, 2008.

[12] A. Henke und S. Frei, „Transient temperature calculation in a single cable using an analytic approach,“ *JFFHMT,* Bd. 7, pp. 58-65, 2020.

[13] S. Önal, M. Kiffmeier and S. Frei, "Modellbasierte intelligente Sicherungen mit umgebungsadaptiver Anpassung der Auslöseparameter," in *EEHE*, Würzburg, Deutschland, 2018.

[14] MathWorks. [Online]. Available: https://de.mathworks.com/help/matlab/ref/pdepe.html. [Accessed 02 03 2021].

[15] Y. J. Han, H. M. Lee and Y.-J. Shin, "Thermal aging estimation with load cycle and thermal transients for XLPE-insulated underground cable," in *IEEE CEIDP*, Fort Worth, TX, USA, 2017.

[16] S. Önal, A. Henke and S. Frei, "Switching strategies for smart fuses based on thermal models of different complexity," in *15th Int. Conf. EVER*, online, 2020.